Structure of Many-Arm Star Polymers in Solvents of Varying Quality: A Molecular Dynamics Study

Gary S. Grest

Corporate Research Science Laboratories, Exxon Research and Engineering Company, Annandale, New Jersey 08801

Received February 1, 1994; Revised Manuscript Received April 11, 1994[•]

ABSTRACT: A molecular simulation of many-arm star polymers in solvents of varying quality is presented. The number of arms f in each star covered the range $3 \leq f \leq 80$ with $N = 50$ and 100 monomers per arm. The resulting equilibrium structures are compared to scaling predictions based on the blob model and to experimental results. The monomer density $\rho(r)$ from the center was found to fall off as a power law, r^{-a}, for both a good and Θ solvent in agreement with the scaling predictions. The free ends were found to be excluded from a region near the center of the star and the distribution of center-to-end distances R was found to be well approximated by a Gaussian for many-arm stars ($f \gtrsim 20$) for all solvents. For small f, there were some deviations from a Gaussian form, particularly for small R. For both a good and Θ solvent, the relaxation time for the shape fluctuations depended imperceptibly on the number of arms f.

I. Introduction

Star polymers are a special class of branched polymers, in which one end of each linear chain is tethered to a small central core to form a single molecule.[1-9] Many-arm stars with a narrow molecular weight (M_W) distribution have been made by chemical reactions with up to 56 arms for polyisoprene[6] and up to 270 arms for polybutadiene.[7] Many of the properties of dilute stars, including the dependence on the size of the star on the number of arms f and number of monomers per arm N and the monomer density profile, are reasonably well understood. The basis for this understanding is due largely to the development of a scaling theory based on the blob model of de Gennes,[10] first applied to star polymers by Daoud and Cotton[11] and Birshtein and Zhulina.[12] This was the first successful theory of a star molecule which included excluded-volume interactions. This picture was later used to understand how end-grafted chains stabilize colloidal particles.[13] Grest *et al.*[14,15] applied this scaling ansatz to determine the form of the static structure function $S(q)$ as well as the relaxation modes of a many-arm star. They found that, in the presence of excluded-volume interactions, there were three typical relaxation processes,[15] in contrast to the independent strand approach of Zimm and Kilb[16] in which there was only one. Strong support for the scaling model comes from a large number of experiments and simulations, though mostly in a good solvent. In a Θ solvent, there remain some unresolved discrepancies in the experimental data. Most of the previous simulations for a Θ solvent have been for relatively small f. Here we consider in more detail the effect of solvent quality on the properties of a star, particularly for large f.

Theoretically, a number of techniques have been applied to study star polymers, including some exact results,[17] series expansion,[18] scaling,[11,12,19] and renormalization group.[20-22] Daoud and Cotton[11] and Birshtein and Zhulina[12] generalized the de Gennes scaling[10] model for linear polymers to star polymers. In this approach, the star consists of three regions, an inner meltlike extended core region, an intermediate region resembling a concentrated solution, and an outer semidilute region. In this outer region, a blob model is used to describe the overall structure of a star. Since the volume accessible to a given chain increases with the distance r from the center of the star, the monomer volume fraction $\rho(r)$ is expected to be a decreasing function of r. Each arm can be seen as a succession of growing spherical blobs. Within one blob each arm behaves as an isolated chain. At a given distance r from the center, a sphere of radius r is cut by f arms. The star looks like a semidilute solution with a screening length $\xi(r)$, where $\xi(r)$ is a function of r and the number of arms f. Each blob contains monomers of a single chain. Since f blobs cover the sphere of radius r, the blob radius is

$$\xi(r) \sim r f^{-1/2} \tag{1}$$

As in any semidilute solution, each blob contains $n(r) \sim \xi(r)^{1/\nu}$ monomers. Here ν is the correlation length exponent, which is 0.588 for a good solvent in three dimension.[23] From this picture, one can easily verify that $\rho(r)$, the number density of monomers, falls off as

$$\rho(r) \sim n(r)/\xi(r)^3 \sim f^{(3\nu-1)/2\nu} r^{(1-3\nu)/\nu} \; (= f^{0.65} r^{-1.30}) \tag{2}$$

Qualitatively, this scaling behavior is nicely illustrated in Figure 1a, in which we present a projection of a typical configuration of a star polymer with $N = 100$ monomers per arm for $f = 20$ in a good solvent. This figure nicely shows the density falloff and corresponding increase in $\xi(r)$ with increasing r, as expected. A similar projection for $f = 10$, 30, and 50 is shown in ref 14 for a good solvent. For the mean-squared average center-to-end distance $\langle R^2 \rangle$ and radius of gyration $\langle R_G^2 \rangle$,

$$\langle R^2 \rangle \sim \langle R_G^2 \rangle \sim N^{2\nu} f^{1-\nu} \tag{3}$$

In a good solvent, $\langle R^2 \rangle \sim N^{1.18} f^{0.41}$. As the solvent quality is decreased and one approaches T_θ, the range over which this result is valid decreases.[24] At T_θ (Figure 1b), each arm can be pictured as a succession of ideal spherical blobs and $n(r) \sim \xi(r)^2$. Equation 2 is replaced by

$$\rho(r) \sim n(r)/\xi(r)^3 \sim f^{1/2} r^{-1} \tag{4}$$

This last result is also valid in the intermediate region, though the crossover from the outer to the intermediate regime has not been observed. In a poor solvent (Figure 1c) the star collapses in on itself as expected.

Dynamical simulations, including molecular dynamics (MD),[14,15] Brownian dynamics,[25] and Monte Carlo (MC)

[•] Abstract published in *Advance ACS Abstracts*, May 15, 1994.

0024-9297/94/2227-3493$04.50/0

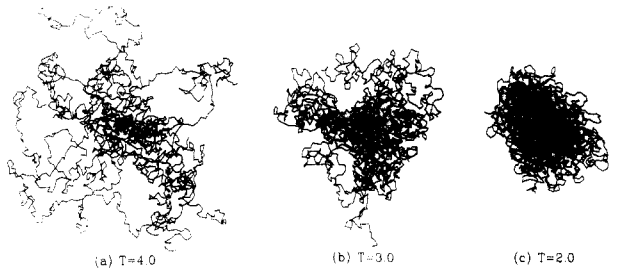

Figure 1. Projection of a typical configuration of a star of f = 20 arms with N = 100 monomers per arm for (a) a good solvent ($T = 4.0\epsilon/k_B$), (b) a Θ solvent ($T = T_\theta = 3.0\epsilon/k_B$), and a poor solvent ($T = 2.0\epsilon/k_B$). These configurations are for an interaction (eq 7) truncated at $r_c = 2.5\sigma$ between nonbonded monomers.

methods,[26-31] have been used to test these scaling predictions and to determine other properties of a star polymer, including the static structure factor[14] in the dilute limit. At present, it is not possible to simulate a melt or even a semidilute solution of many-arm star polymers due to the long relaxation times. For few-arm stars ($f \lesssim 12$) MC methods are very efficient, while for a large number of arms, MD methods work very well. For small f, the density of monomers of the star is low almost everywhere and static MC methods in which one generates the chains by constructing walks is probably the most accurate method for static properties.[32-37] Dynamic MC also works well in this limit, particularly if one invokes nonlocal moves.[28] While the recently introduced configurational biased MC method[38] has not been applied to star polymers, it should also be efficient. However, as f increases, the interior becomes very dense and many of these methods fail or become inefficient. In this case, it is more useful to use either MD methods, as is done here, or a local stochastic MC method such as the bond fluctuation method on a lattice[39] or a simple off-lattice MC in which one attempts to move one monomer at a time.[40] For dynamics, only those methods which use local moves, either using MC or MD, can be used. However, neither of these latter two methods has been used to study many-arm stars in either good or Θ solvent. For a review of simulation methods appropriate for stars and other tethered systems, see ref 41.

Here I present the results of an extensive MD simulation of many-arm stars, with $3 \le f \le 80$ for n = 50 and 100 monomers per arm in solvents of varying qualities. In a good solvent, these results for longer chains than have been typically studied are in agreement with previous simulations, experiments, and scaling theory. Results for the mean-squared radius of gyration $\langle R_G^2 \rangle$, normalized by $\langle R_{G1}^2 \rangle$, the mean-squared radius of gyration of a linear polymer of length equal to that of an arm, are universal and satisfy the scaling prediction (eq 2) for $f \gtrsim 10$. Results for the center-to-end distance of the free end clearly show that the ends are excluded from a region near the center, in agreement with the predictions based on the Daoud–Cotton scaling model[15] and the recent variational approach of Li and Witten.[42] This is in contrast with a polymer brush in which one end is grafted to a flat surface. In this case there is no exclusion zone for the free ends.[43] For a star polymer in a very good solvent, the distribution $P(R)$ is fit nearly perfectly by a Gaussian for large $f \gtrsim 20$. As the solvent quality is reduced, for large f, small deviations from a Gaussian are observed. For smaller f, $P(R)$ deviates somewhat from a Gaussian form even for a very good solvent, particularly for small R, though the deviations are not that large. This Gaussian form for $P(R)$ is in agreement with earlier theoretical predictions based on the scaling model by Grest *et al.*[15] The form factor, $P(q)$, for stars in dilute solution is determined for both a good and Θ solvent. Finally, the relaxation of the shape fluctuations is shown to be imperceptibly dependent on the number of arms f for both a good and Θ solvent, as suggested earlier by scaling theory.[15] While some of the results presented here for a good solvent follow from earlier studies, this is the first systematic study of the properties of many-arm stars ($f > 12$) for solvents of varying qualities. Most of the previous studies have been for $f \ge 6$, though Batoulis and Kremer[36] and Zifferer[29] have studied stars with $f \le 12$ and Freire *et al.*[27] those with f = 6, 12, and 18 at the Θ point.

The outline of the paper is as follows. In section 2, the simulation method and model are briefly described. In section 3, results for an isolated star in good solvent are presented and compared to the predictions of scaling theory and experiments on several polymers. Results for the distribution of center-to-end distances, $P(R)$, are presented and discussed in some detail. In section 4, results for a Θ and poor solvent are presented, while in section 5, relaxation of a star is discussed. Finally, a brief summary of the main results is given in section 6.

II. Model and Method

The equilibrium structure of the stars in a solvent was obtained using a molecular dynamics method in which each monomer is coupled to a heat bath. The equation of motion for monomer i (of mass m) is given by

$$m\frac{d^2\mathbf{r}_i}{dt^2} = -\nabla U_i - m\Gamma\frac{d\mathbf{r}_i}{dt} + \mathbf{W}_i(t) \tag{5}$$

where Γ is the friction coefficient that couples the monomers to the heat bath. The random force coming from the monomer–heat bath coupling is given by a white-noise term $\mathbf{W}_i(t)$, which satisfies

$$\langle \mathbf{W}_i(t)\cdot\mathbf{W}_j(t')\rangle = 6k_BTm\Gamma\delta_{ij}\delta(t-t') \tag{6}$$

Here k_B is the Boltzmann constant and T is the temperature. The potential U_i is composed of two terms: $U_i = U^0 + U^{ch}$. U^0 is a Lennard-Jones (LJ) potential

$$U^0 r = \begin{cases} 4\epsilon\,[(\sigma/r)^{12} - (\sigma/r)^6 - (\sigma/r_c)^{12} + (\sigma/r_c)^6] & \text{if } r \le r_c \\ 0 & \text{if } r > r_c \end{cases} \tag{7}$$

In our previous studies of the stars,[14,15] $r_c = 2^{1/6}\sigma$, such that the potential is purely repulsive. This is an efficient model for studying good solvent conditions. Since the potential is close to a hard sphere, this case is referred to as athermal or a very good solvent for convenience. To introduce the effect of solvent quality, the range of the interaction is extended to $r_c = 2.5\sigma$. Thus, by changing T, the relative importance of the monomer–monomer attraction could be varied and the effective quality of the solvent changed without explicitly introducing solvent monomers. For the potential parameters used here, $T_\theta = 3.0 \pm 0.1\epsilon/k_B$.[44]

While U^0 acts between all pair of monomers, the second interaction U^{ch} is an attractive potential binding the monomers along a chain or to the central sphere.[14,44] The strength of the attractive potential was linearly dependent on temperature T so that bond length l would be essentially independent of T.[44] It had a value of about 0.97σ.

The equations of motion[45] of the monomers are integrated using a velocity–Verlet algorithm with a time step Δt, taken to be as large as possible, while keeping the integration stable. I used $\Delta t = 0.012\tau$ for the good solvent case and 0.006–0.008τ for T in the vicinity of T_θ, where $\tau = \sigma(m/\epsilon)^{1/2}$. The larger T is, the smaller is Δt. The friction coefficient Γ was set to be $\Gamma = 0.5\tau^{-1}$. We used units in which $m = \sigma = 1$ and measured the temperature in units of ϵ/k_B. Further details on the simulation technique can be found elsewhere.[46]

Using this method, stars consisting of N monomers per arm, with N = 50 and 100 for $3 \le f \le 80$, were simulated. The first monomer of each chain is firmly attached to a small sphere of radius R_c which was fixed in space at the origin. The radius of

Table 1. Properties of Many-Arm Stars in Good Solvent[a]

f/N	T_t/τ	$\langle R_G^2\rangle$	$\langle R_{Ga}^2\rangle$	$\langle R^2\rangle$
1/50	80 000	23.5		154.2
3/50	24 000	69.6	23.9	173.9
6/50	30 000	89.4	25.0	195.0
10/50	28 000	104.9	25.7	219.6
20/50	26 000	130.1	29.5	255.9
30/50	14 000	149.1	29.3	292.4
40/50	24 000	162.2	30.8	313.9
50/50	24 000	176.3	32.1	340.5
1/100	120 000	55.2		179.3
3/100	48 000	149.1	56.6	386.0
4/100	60 000	198.5	61.9	455.8
6/100	84 000	207.2	60.0	451.6
10/100	120 000	249.9	62.5	515.1
20/100	36 000	288.2	66.0	561.8
30/100	42 000	335.5	69.5	644.7
50/100	21 600	405.0	75.9	771.3
64/100	24 000	443.5	78.8	835.1

[a] Monomers interact with a purely repulsive potential ($r_c = 2^{1/6}\sigma$ in eq 7). f is the number of arms, N is the chain length in each arm, T_t is the total duration of the run after equilibration, $\langle R_G^2\rangle$ is the mean-squared radius of gyration of the entire star, $\langle R_{Ga}^2\rangle$ is the radius of gyration of a single arm, and $\langle R^2\rangle$ is the mean-squared center-to-end distance. All simulations were run at $T = 1.2\epsilon/k_B$.

Table 2. Properties of Many-Arm Stars as a Function of Temperature[a]

f/N	T_t/τ	k_BT/ϵ	$\langle R_G^2\rangle$	$\langle R_{Ga}^2\rangle$	$\langle R^2\rangle$
1/100	70 000	4.0	35.3		218.7
3/100	30 000	4.0	90.0	35.8	227.5
6/100	30 000	4.0	127.0	39.3	273.5
10/100	30 000	4.0	144.8	41.2	300.5
20/100	18 000	4.0	177.1	42.3	331.4
30/100	12 000	4.0	199.5	43.7	373.0
50/100	3 000	4.0	236.7	46.6	432.8
1/100	64 000	3.0	29.8		180.6
2/100	240 000	3.0	58.3		172.5
3/100	210 000	3.0	66.5	28.5	172.0
4/100	140 000	3.0	77.8	29.9	174.4
5/100	84 000	3.0	80.0	29.8	180.9
6/100	147 000	3.0	80.8	29.2	175.8
8/100	42 000	3.0	94.8	30.6	195.8
10/100	84 000	3.0	101.1	30.7	199.3
20/100	28 000	3.0	120.8	32.4	221.1
30/100	14 000	3.0	135.9	32.1	238.2
50/100	5 600	3.0	167.9	34.3	287.6
6/100	4 000	2.0	29.1	16.4	59.6
10/100	4 000	2.0	38.0	17.9	73.5
20/100	4 800	2.0	56.7	18.4	84.7
30/100	4 000	2.0	69.3	20.4	102.1

[a] Parameters are the same as in Table 1, except the range of interaction in eq 7 has been extended to $r_c = 2.5\sigma$.

this sphere was chosen to be as small as possible. For small f, $R_c = 0.5\sigma$, while for large f, R_c was increased to accommodate the large number of arms. For $f = 50$, $R_c = 1.25\sigma$. Since R_c is significantly smaller than the average center-to-end distance R, the arms can be considered to be attached to a point. In our previous simulation,[14,15] the central site was allowed to move and the star diffused subject to Rouse dynamics. However, since the overall diffusion of the star is quite small for large f and N ($D \sim 1/fN$), D could not be measured accurately. In the present simulations, the central sphere to which the arms are attached is fixed in space and hence the rotation or translation diffusion constant is zero. The simulations are initialized by simply growing the chains as random walks, letting the chains overlap in the initial configuration. They are then equilibrated with a softer core potential until all the excluded-volume conditions are satisfied and the full Lennard-Jones interaction could be switched on.[14]

After a long equilibration run (typically (2–5) × $10^5\Delta t$), extremely long runs were made as indicated in Table 1 for $r_c = 2^{1/6}\sigma$ for $N = 50$ and 100 and Table 2 for $r_c = 2.5\sigma$ for $N = 100$. Additional runs for $N = 50$ including an $f = 80$-arm star for $r_c = 2.5\sigma$ were also made. The runs are typically more than a factor of 10 longer than those presented in ref 14 for the athermal case

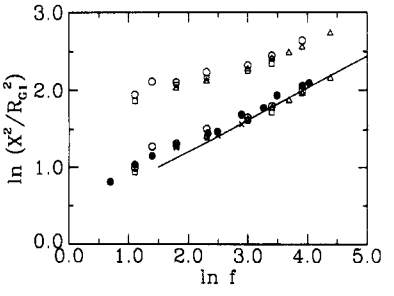

Figure 2. Radius of gyration $\langle R_G^2\rangle/\langle R_{G1}^2\rangle$ (lower curve) and average squared end-to-end distance $\langle R^2\rangle/\langle G_1^2\rangle$ (upper curve) versus f for a good solvent. $\langle R_{G1}^2\rangle$ is the mean-squared radius of gyration for a single polymer chain of a length of one of the arms. The solid circles are data for polystyrene and polyisoprene from ref 6. The crosses are from the off-lattice MC simulations of Freire *et al.*[27] for $N = 49$ or 55. The other symbols are from MD simulations for monomers interacting with a purely repulsive Lennard-Jones interaction, (eq 7), at $T = 1.2\epsilon/k_B$ for $N = 100$ (○) and at $T = 4.0\epsilon/k_B$ for $r_c = 2.5\sigma$ for $N = 50$ (△) and $N = 100$ (□). The solid linear has slope of 0.41.

and many times longer than the relaxation time for the shape fluctuations discussed in section IV. This was particularly important for $T = 3.0$ where the relaxation was slow. Every 100–200Δt a number of quantities were calculated and saved for later analysis. These included the center-to-end distance R of the each arm, the squared radius of gyration of the each arm

$$R_{Ga}^2 = \frac{1}{N}\sum_{j=1}^{N}(\mathbf{r}_{i,j} - \mathbf{r}_{i,CM})^2 \tag{8}$$

and the radius of gyration R_G^2 of the entire star. Here $\mathbf{r}_{i,j}$ is the position of monomer j on arm i and $\mathbf{r}_{i,CM}$ is the center of mass of arm i.

From these quantities, the mean-squared averages of each, the distribution $P(R)$ of center-to-end distances and various autocorrelation functions were calculated. Due to the long runs, the statistical errors in $\langle R^2\rangle$ and $\langle R_G^2\rangle$ are relatively small, of order 1–2%. In addition, the monomer density $\rho(r)$ and the static form factor $P(q)$ was also calculated. $P(q)$ is given by

$$P(q) = \frac{1}{fN}\left\langle \sum_{ij} \exp^{i\mathbf{q}\cdot(\mathbf{r}_i - \mathbf{r}_j)} \right\rangle \tag{9}$$

where the sum is over all monomers in the system. In order to obtain good statistics 20–30 $\mathbf{q}$ vectors were chosen randomly from a sphere of radius $|\mathbf{q}|$ for each configuration, taken 10 000 to 20 000Δt apart.

III. Good Solvent

In a good solvent, the results from various groups[14,15,18,25–35] agree very well, though most of these are for small f. As an example, results for $\langle R_G^2\rangle/\langle R_{G1}^2\rangle$ and $\langle R^2\rangle/\langle R_{G1}^2\rangle$, where $\langle R_{G1}^2\rangle$ is the radius of gyration for a single polymer chain of N monomers, are shown in Figure 2. The off-lattice MC simulations of Freire *et al.*[27] are also presented. Experimental results for polystyrene and polyisoprene[6] are also shown. Note that by normalizing $\langle R_G^2\rangle$ by $\langle R_{G1}^2\rangle$ for a chain of a length of one arm, the results for both the simulations and experiment fall on the same curve. By dividing out of the single chain radius of gyration, one can compare results from different simulations as well as different experiments. Even though both simulations were carried out for coarse-grained models, in which no local bending and torsion terms were included, the simulations describe the experimental results very well. As expected from the scaling theories, the global properties of the star are universal. The solid line in Figure 2 indicates the predicted asymptotic power, 0.41. Note that the limiting scaling form is reached very early. The monomer density profile $\rho(r)$ scaled by $f^{0.65}$ is shown in Figure 3a for four values of f from 4 to 50 for $N = 100$. The

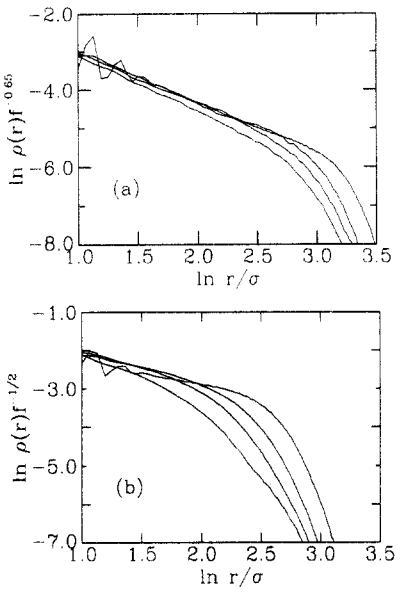

Figure 3. log–log plot of the density $\rho(r)$ scaled by $f^{(3\nu-1)/2\nu}$ versus r/σ for the $f = 50, 20, 10$, and 4 arm stars with $N = 100$ monomers per arm for (a) a very good solvent and (b) a Θ solvent. The larger f is, the further the curves extent in r. The good solvent results are for $T = 1.2\epsilon/k_B$ for a purely repulsive Lennard-Jones interaction (eq 7) truncated at $r_c = 2^{1/6}\sigma$. The Θ solvent results are for $T = T_\theta = 3.0\epsilon/k_B$ for $r_c = 2.5\sigma$.

measured slope is 1.30 ± 0.03 for $f \geq 10$, in excellent agreement with the expected value 1.30. Note surprisingly the results for $f = 4$ deviate slightly from the scaling predictions as was already seen in Figure 2. The oscillations for small r for $f = 50$ come from the packing of spheres near the tethering point. The rapid decay for large r is due to the finite chain length. The results clearly scale with $f^{0.65}$ in agreement with the scaling prediction and the earlier MD simulations of Grest *et al.*[14] for shorter chains, $N = 50$. Batoulis and Kremer[35] found a similar scaling for $3 \leq f \leq 6$. Using a self-consistent-field (SCF) model, Dan and Tirrell[47] and Wijmans and Zhulina[48] found that $\rho(r)$ scaled as predicted by eq 2. For the stars simulated here, the scaling is valid even at very short distances from the center, indicating that the simulations clearly exhibit the scaling predicted for a swollen star and there is no need to consider the core regime. This core region is important for micellar stars and for chains grafted onto a small colloidal particle.

Because the interior of the star can become quite dense as f increases, one would expect that the free end of the chain is excluded from the core reason by simple steric effects. The expected width of the distribution $P(R)$ of center-to-end distances R can be estimated from the scaling model,[11,12] by considering[15] the distance R of a chain confined in a narrow cone of opening $\theta = 2f^{-1/2}$, since a cone subtends a solid angle which is $1/f$ of the sphere. The center-to-end distance of such a chain fluctuates as though it were confined in a straight tube of diameter $R\theta$. The free energy of this chain, relative to an unconfined chain, is of order $k_BTR/(R\theta)$ or k_BT per blob of size $R\theta$. Decreasing R to zero costs a further energy of this order. Thus the free energy associated with a small fluctuation ΔR of R away from its average value is of order $k_BTR/(R\theta)[\Delta R/R]^2$. Thus thermal fluctuations in ΔR, of energy $\sim k_BT$, are expected to be of order $\langle R\rangle\theta^{1/2} = 2^{1/2}\langle R\rangle f^{-1/4}$. For $f \gg 1$, $P(R)$ should approach a Gaussian shape of width $\Delta R \ll \langle R\rangle$. For small r, Ohno and Binder[19] found that, in the scaling limit $P(R) \sim (R/\langle R\rangle)^{\theta(f)}$, where $\theta(f)$ is related to the exponent $\gamma(f)$. For large f, $\theta(f) \sim f^{1/2}$ in three dimensions,[19] and $P(R)$ will appear to have an exclusion zone, although strictly speaking it does not. Li and

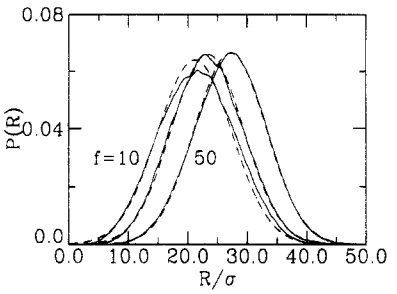

Figure 4. Distribution function $P(R)$ for the center-to-end distances versus R for a star with $f = 10$, 20, and 50 arms for $N = 100$. The simulations are for the purely repulsive interaction truncated at $r_c = 2^{1/6}\sigma$ for $T = 1.2\epsilon/k_B$. The solid line is the raw data, while the dashed line is a Gaussian with the same width and standard deviations as the data.

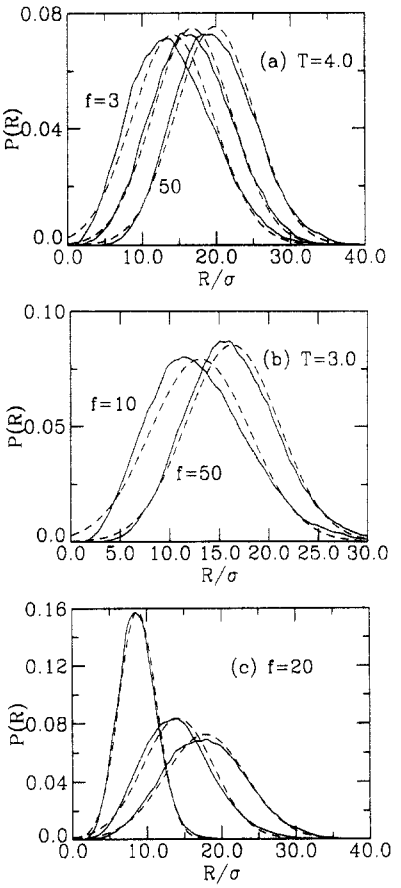

Figure 5. Distribution function $P(R)$ for the center-to-end distances versus R for a star (a) in a good solvent ($T = 4.0\epsilon/k_B$) with $f = 3$, 10, and 50 arms, (b) in a Θ solvent ($T = T_\theta = 3.0\epsilon/k_B$) for $f = 10$ and 50, and (c) for $f = 20$ for three temperatures $T = 2.0$, 3.0, and $4.0\epsilon/k_B$ (from left to right) for $N = 100$. The simulations are for the interaction (eq 7) truncated at $r_c = 2.5\sigma$. The solid line is the raw data, while the dashed line is a Gaussian with the same width and standard deviations as the data.

Witten[42] used a variational approach to minimize the free energy with respect to the free and distribution and the stretching profiles of the polymer chains. Their calculations predict a very large exclusion zone for the free ends and a very different functional form for $P(R)$. In the limit of large f, the free ends would be restricted to the last 6% of the layer height and $P(R)$ would not be Gaussian.

Results for $P(R)$ for a 10-, 20-, and 50-arm star in a very good solvent are shown in Figure 4. In Figure 5a similar results are shown for $f = 10$ and 50 at a temperature about 30% above T_θ. All of these results are for $N = 100$. Note that, in both cases, $P(R)$ is well approximated by a Gaussian, which corresponds to the dashed lines in these figures. Note that these are not best fits to a Gaussian form but simply a plot of a Gaussian function with the

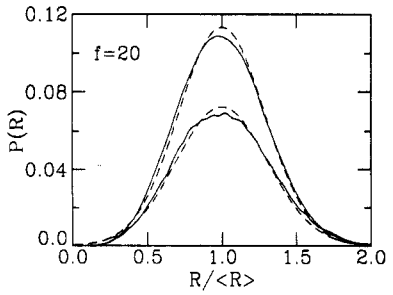

Figure 6. Distribution function $P(R)$ for the center-to-end distances versus R for a star in a good solvent ($T = 4.0\epsilon/k_B$) with $f = 20$ arms for $N = 50$ (upper curve) and 100 (lower curve). The solid line is the raw data, while the dashed line is a Gaussian with the same width and standard deviations as the data.

same mean and standard deviation as the measured distributions. For large-arm stars ($f \gtrsim 20$) in a very good solvent (purely repulsive potential), $P(R)$ fits a Gaussian form almost perfectly. This is in agreement with earlier results of Grest *et al.*[15] for $N = 50$. As the solvent quality is lowered or the number of arms is reduced (Figure 5a), there are some deviations from a Gaussian form. The distribution is approximately symmetric, shifted slightly toward the center. For small f, the Gaussian overestimates the number of free ends near the center, suggesting that part of the deviation is due to finite size effects and the deviations may become less for longer arms. In Figure 6, results for $f = 20$ for $T = 4.0\epsilon/k_B$ for $N = 50$ and 100 are shown, clearly indicating the general form of $P(R)$ is independent of N. These results are in agreement with the numerical SCF calculation of Wijmans and Zhulina[48] for polymers attached to the surface of a highly curved sphere.

While the center of the distribution is clearly dependent on the number of arms, the absolute width is only weakly dependent on f. It depends mostly on the solvent quality and N. Thus the relative width decreases roughly as $1/\langle R\rangle \sim f^{-0.2}$. This behavior is consistent with our earlier simulations. It is also consistent with the simple theoretical arguments,[15] discussed above, which are based on the Daoud–Cotton model of a star. More recent theoretical work by Li and Witten[42] indicates that the relative width of the end distribution does not decrease to zero but reaches a finite asymptote of about 6%. Since the observed widths are much larger than this, we would need arm numbers several times larger than those used here to approach the predicted relative width. It is also important to note that for a highly curved cylinder, where they were able to also solve the SCF equations exactly, the size of the exclusion zone decreased significantly compared to the variational approach. In addition the variational approach appears to work less well as the dimension of the surface being tethered to decreases presumably because the strong stretching ansatz which they use is not as applicable. Thus this lack of agreement is not too surprising. If the theory is correct, it applies only when the number of arms is very large. The lack of agreement between the theory and the earlier simulations is definitely not a finite chain-length effect as they suggested. Finally, because many arms are attached to a central core, steric effects which are not included in these calculations must play an important role. Thus, while the scaling theory is clearly an oversimplification, it describes the distribution of the free end very well for f in the range often studied experimentally.

Experimentally, small-angle neutron scattering[49-53] is a useful way to determine not only the size of the star but also something about its internal structure. The measured scattering intensity, $I(q)$, as a function of the scattering wave vector $q = 4\pi/\lambda \sin(\theta/2)$, where λ is the incident neutron wavelength and θ is the scattering angle, can be represented by the product $S(q)P(q)$. Here $S(q)$ represents the interparticle structure factor determined by the interaction potential between the star molecules, while $P(q)$ represents the form factor of the individual stars determined by the structure of the star. In a dilute solution, the interactions between stars can be neglected, $S(q) = 1$ and the intensity $I(q) \sim P(q)$. Usually $P(q)$ is determined by selectively labeling a small fraction of the stars so that $S(q)$ can then be deduced from $I(q)/P(q)$. $P(q)$ can also be determined from the simulations. Note that in most papers on polymers the intra- and interparticle correlations are not separated and are simply referred to as the structure factor $S(q)$ which is proportional to $I(q)$. For a star, as discussed in ref 14, there are at least three characteristic lengths which must be considered: the radius R of the star, the correlation length ξ_{max} of the largest blob, and the monomer size σ. For $qR < 1$, $P(q)$ has the normal Guinier behavior: $P(q) = Nf[1 - q^2\langle R_G^2\rangle/3 + \mathcal{O}(q^4\langle R_G^2\rangle^2)]$. For $\xi_{max}^{-1} < q < \sigma^{-1}$, the scattering can be understood by covering the polymer with spheres of radius q^{-1}. In the absence of strong correlations between the positions of the spheres, these scatter incoherently. The resulting scattering intensity $NfP(q)$ is the number of spheres times the structure factor of a single sphere. In the star, the majority of these imaginary spheres are contained within blobs much larger than the spheres. The correlations between spheres are thus nearly the same as in a simple excluded volume of polymer. This gives a fractal scattering law $P(q) \sim q^{-1/\nu}$, independent of f and N. In between these two limits, $P(q)$ must fall from about Nf to about $(\xi_{max}/\sigma)^{1/\nu}$. While the simpliest way to connect these two regimes is by a power law decay q^{-d}, the actual scattering is more complex.[14] In this regime, q^{-1} is larger than the largest blob, and the polymer chain structure is invisible to the scattering. The dominant scattering is from the relatively sharp (see Figure 1) outer boundary of the star, which gives rise to a faster decrease in the scattering envelope, q^{-d-1}. For large f, oscillations superimposed on this Porod envelope should also be seen. Results for $P(q)$ are shown in Figure 7a for a star polymer in a good solvent with $N = 100$ for four values of f. The results are in good agreement with this picture. For large f, the oscillations in $P(q)$ are apparent. For high q, one finds the expected scaling of $P(q)$, though the observed ν is weakly dependent on f for this chain length. For $f = 4$, the observed slope is approximately 1.66 ± 0.05, very close to the expected value $1/\nu = 1.70$, while for large f, the observed slope is somewhat smaller, $\nu = 1.53 \pm 0.05$. The value of the slope depends partially on exactly what q range is fit. Due to the larger core region, the size of the scaling region for this chain length is limited for large f. It is expected that, for larger N, the slope will increase.

IV. Θ and Poor Solvent

At the Θ point, the self-repulsion of the monomers, due to the excluded volume, is just compensated for by the interactions with the solvent. While this tricritical point is well understood for linear chains, less is known about the properties of stars at T_θ. Candau *et al.*[54] assumed that at T_θ all the arms can interpenetrate each other completely. This means that all virial coefficients vanish and the size of the star is given by the Zimm–Stockmayer[55] equation,

$$g(f) = \lim_{N\to\infty} \frac{\langle R_G^2\rangle}{f\langle R_{G1}^2\rangle} = (3f - 2)/f^2 \qquad (10)$$

While this is obviously an oversimplification, it turns out

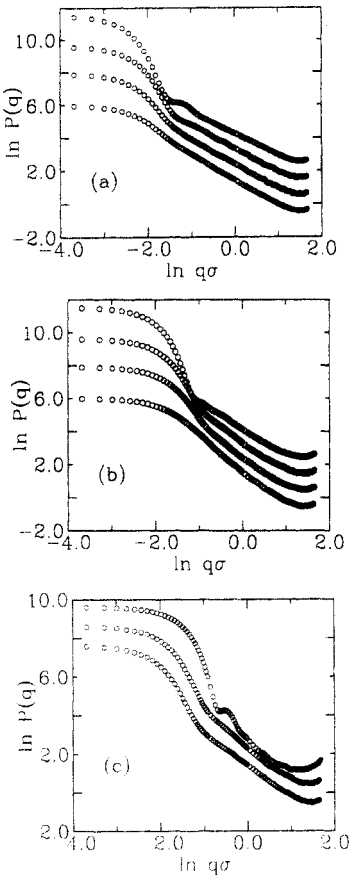

Figure 7. $P(q)$ versus $q\sigma$ for a star (a) in a very good solvent ($T = 1.2\epsilon/k_B$, $r_c = 2^{1/6}\sigma$) for $f = 4$, 10, 20, and 50 arms (from bottom to top, each curve is displaced vertically for clarity), (b) in a Θ solvent ($T = T_\theta = 3.0\epsilon/k_B$) for the same values of f, and (c) for $f = 20$ for three temperatures $T = 2.0$, 3.0, and $4.0\epsilon/k_B$ (from top to bottom, also displaced for clarity) for $N = 100$.

Table 3.[a] g Values for $T = T_\theta$

f	RW^b	MC^c	MD^d	PS^e	PI^f
3	0.778	0.79	0.74	0.76	
4	0.625	0.68	0.65	0.63	0.69
5	0.520	0.55	0.54		
6	0.444	0.48	0.45	0.45	0.47
8	0.344	0.39	0.40		0.44
10	0.280		0.34		0.42
12	0.236	0.28		0.27	0.37
18	0.160			0.22	0.29
20	0.145		0.20		

[a] Where available, g was determined from extrapolations for large molecular weight when possible; otherwise, the data for the longest arms were used.[36] [b] Random walk (eq 10).[55] [c] Monte Carlo results of Batoulis and Kremer.[36] [d] Molecular dynamics results for $T = T_\theta = 3.0\epsilon/k_B$ for $N = 100$. [e] Polystyrene (PS) results for $f = 4$ and 6 from ref 2 and for $f = 3$, 12, and 18 from ref 3. [f] Polyisoprene (PI) results from ref 6.

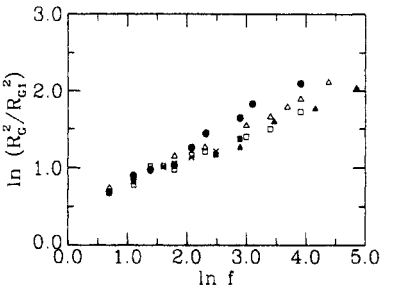

Figure 8. Radius of gyration $\langle R_G^2\rangle/\langle R_{G1}^2\rangle$ versus f for a Θ solvent. The solid circles are for polyisoprene in dioxane,[6] the solid squares are for polystyrene in cyclohexane,[3] and the solid triangles are for polybutadienes in dioxane.[4,8,9] The crosses are from the MC simulations of Batoulis and Kremer[36] extrapolated to large N. The open triangles ($N = 50$) and squares ($N = 100$) are from the present MD simulations in which nonbonded monomers interact with a Lennard-Jones interaction (eq 7) cutoff at $r_c = 2.5\sigma$ for $T = T_\theta = 3.0\epsilon/k_B$.

to work quite well. As seen from eq 4, the Daoud and Cotton scaling argument gives $g(f) \sim f^{-1/2}$. However, since at T_θ the second virial coefficient between a pair of arms vanishes, a third arm still gives a repulsive interaction.[12] Batoulis and Kremer[36] have argued that, because of this effect, two, but not more than two, arms of the star can share a blob of diameter $\xi(r)$ at T_θ and one needs more arms than in a good solvent to observe the Daoud–Cotton scaling. They estimated that the random-walk (RW) results (eq 10) should cross over to the scaling result for $5 \le f \le 10$.

To study the importance of three-body interactions on stars, Batoulis and Kremer[36] carried out high-precision MC simulations of linear and star polymers on the fcc lattice for $1 \le f \le 12$ and $N \le 900$ using the inverse-restricted sampling method.[56] These simulations, extended earlier simulations on smaller stars by Mazur and McCrackin.[32] They found that T_θ was independent of f for $N \to \infty$. Similar results were found experimentally for polyisoprene stars in dioxane[6] where the temperature at which the second virial coefficient A_2 vanishes for small f and N is lower than T_θ for a linear chain but increases as N increased. In the limit of large M_W, T_θ for the star is the same as that for a linear chain.

The g-factor obtained from the present MD simulations, lattice MC simulations,[36] and experiment is compared to the RW result in Table 3.[36] Since the Θ point is only known approximately for the present model, the MD results are probably not as accurate as the lattice MC results[36] for small f. The experimental data in Table 3 are for polystyrene[3] in cyclohexane and polyisoprene[6] in dioxane. Results from the off-lattice MC simulations of Freire *et al.*[27] for $f = 6$ and 12 also agree very well with the two simulations listed, while their results for $f = 18$ are somewhat too low. Zifferer[29] found $g = 0.640$, 0.385, and 0.285 for $f = 4$, 8, and 12, respectively, using a pivot algorithm on the tetrahedral lattice. For small f the RW result gives a reasonable approximation for g, though for larger f the RW result underestimates the size of the star. Note that all of these results are in contrast with those of Bruns and Carl,[37] who interpret their MC results in terms of an f-dependent Θ point and, at least for $4 \le f \le 6$, g is within their numerical accuracy essentially the same as the RW result. For $f \gtrsim 8$ the polyisoprene data deviate significantly from both the simulations and the polystyrene data. The reason for this difference is unclear. In Figure 8, $\langle R_G^2\rangle/\langle R_{G1}^2\rangle$ is plotted versus f for a wider range of f. Experimental data for polybutadiene[4,8,9] are also shown. As shown in Table 3 for small $f \lesssim 8$, the results for all three experimental systems agree reasonably well with both the MC and MD results, though for large f the results from the three experiments and the simulations scatter significantly. The polyisoprene data can be fit reasonably well with the scaling form over the entire range of f, while the polystyrene and polybutadiene data as well as the MD results suggest that scaling can only be reached for much larger values of f. This is in contrast to good solvent results where the data for different experimental systems agree very well. The disagreement for this supposedly universal value between the three data sets is surprising and unexplained. Some of it may be due to finite chain-length effects as seen in the simulation results for $N = 50$ and 100 and from the uncertainty in the Θ temperature for both the simulation and experiment.

The monomer density profile $\rho(r)$ scaled by $f^{1/2}$ is shown in Figure 3b for four values of f from 4 to 50. The results for $f = 10$ and 20 scale as expected with f and decay with

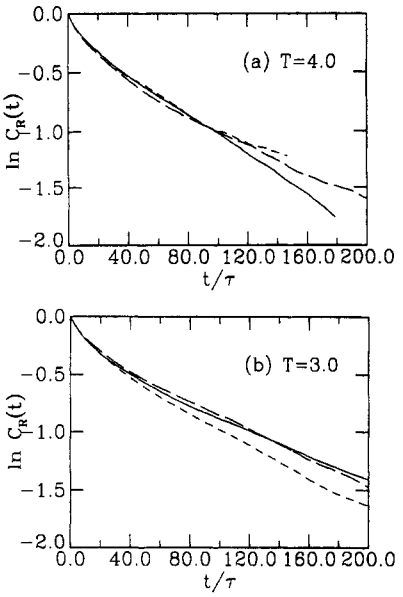

Figure 9. Autocorrelation function $C_R(t)$ for the center-to-end distance R for three stars, $f = 10$ (long dashed), 20 (solid), and 50 (short dashed) for (a) a good solvent at $T = 4.0\epsilon/k_B$ and (b) a Θ solvent ($T = T_\theta = 3.0\epsilon/k_B$). Both are for the case in which the monomers interact with a Lennard-Jones interaction (eq 7) truncated at $r_c = 2.5\sigma$.

a power law consistent with r^{-1} as predicted by scaling theory. However, there are deviations from this behavior for both $f = 4$ and 50. For small f, as in the good solvent, the decay is somewhat faster. The number of arms is too small for scaling theory to hold. For large $f = 50$, the monomer density is quite large over most of the region, leading to very small blobs and deviations from the simple scaling approach. As in the good solvent, the rapid decay for large r is due to the finite chain length.

The distribution of free ends for a Θ solvent is shown in Figure 5b. As for $T = 4.0\epsilon/k_B$, the distribution is approximately symmetric, with a slight shift toward the center of the star. The Gaussian form is a very good fit for large f but deviates for small f, where it overestimates the number of free ends near the origin, as seen for $f = 10$ (Figure 5b). In Figure 5c results for varying solvent qualities are compared for $f = 20$. Note that, even for a poor solvent ($T = 2.0\epsilon/k_B$), the Gaussian fits very well.

The form factor $P(q)$ is shown for $T = T_\theta$ in Figure 7b. For small f, $P(q)$ scales like q^{-2} as expected for a Θ solvent. For large f, as in a good solvent, the scaling regime is rather limited for these chain lengths, and $P(q)$ decays more slowly. The effective slope for high q is 1.6 ± 0.1. For larger N, this slope is expected to increase for large f. In Figure 7c, results for $P(q)$ for varying solvent qualities are compared for $f = 20$. The scattering from the sharp interface in the poor solvent is clearly seen even for $f = 20$.

V. Relaxation of Star Polymers

The scaling picture of a star can also be used to predict its dynamic relaxation processes.[15] There are at least three qualitative distinct relaxation processes for a star, which occur on different time scales and only weakly coupled to each other. While all three of these mechanisms also occur for linear polymers, in a star they are easily separable.

First the star relaxes via an overall shape fluctuation or elastic modes. This time scale is that of cooperative diffusion over the star size R. A second process is rotation diffusion of the object. For linear polymers, these first two have the same relaxation time, up to constants of order unity. However, for large f, the shape fluctuations relax progressively faster. Hence, these two processes are expected to have the same dependence on N but a different dependence on f. The rotational diffusion is slower since it is not enhanced by the pressure within the star, as the elastic modes are. The third process and by far the slowest is the disentangling of two or more interwined arms. Such a configuration can easily survive the shape or rotational relaxations. The larger f is, the better one can distinguish these processes. If excluded-volume interactions are ignored, as done by Zimm and Kilb[16] in the first study of the dynamics of branched polymers, then these three different relaxation mechanisms could not have been distinguished. In the present simulation, since the central monomer is fixed in space, there is no translational diffusion in this case. Also since the ends are attached to specific sites on the surface, there is no rotational diffusion as well. These processes as well as the disentanglement process were studied in ref 15. Here only the fastest processes, the shape fluctuations, are examined, to test the scaling, particularly at T_θ.

The shape fluctuations can be measured directly by studying the fluctuations of the inertia tensor $\mathbf{M}$, where $\langle R_G^2 \rangle = \langle M_{xx} + M_{yy} + M_{zz} \rangle$. The typical shape fluctuations are then given by the time autocorrelation function of the elements of $\mathbf{M}$, R_G^2, R_{Ga}^2, or R^2.[14,15,30,31] For example, the autocorrelation function of $C_R(t)$ is defined by

$$C_R(t) = (\langle R(t)\, R(0) \rangle - \langle R \rangle^2)/(\langle R^2 \rangle - \langle R \rangle^2) \quad (11)$$

Grest *et al.*[15] worked out a prediction for the scaling of $C_R(t)$ by considering the fluctuations in R for a single arm. The fluctuations in the total length arise from independent fluctuations of order ξ within each blob. Thus R fluctuates by an amount of order $\xi(R/\xi)^2$. For a star, the largest length available is given by the size of the largest blob, which has a diameter $\xi_{max} \sim Rf^{-1/2}$. The bulk of the monomers is to be found in this largest blob.[11,12] Thus, the relative amplitude of the fluctuations in $\langle R^2 \rangle$ falls off as $\xi_{max}/R \sim f^{-1/2}$. The longest relaxation time τ_B of such a local fluctuation is given by the Rouse time of an isolated chain of $n_{B,max}$ monomers, $\tau_B \sim \xi_{max}^2 n_{B,max}$, where $n_{B,max} \sim \xi_{max}^{1/\nu}$. In the scaling picture, $n_{B,max} \sim Nf^{-1/2}$ and thus $\tau_B \sim (Nf^{-1/2})^{1+2\nu}$. This describes the initial stage of the local relaxation. In order to produce an overall shape fluctuation, a density fluctuation must diffuse a distance on the order of the diameter of the star, which is R. The diffusion constant for a semidilute solution is given by ξ^2 divided by the local relaxation time τ_B. Thus τ_{el} is of order

$$\tau_{el} \sim \tau_B(R/\xi_{max})^2 \sim N^{1+2\nu} f^{1-(1+2\nu)/2} \quad (12)$$

In a good solvent, $\tau_{el} \sim N^{2.18} f^{-0.09}$, while at the T_θ, $\tau_{el} \sim N^2 f^0$. Thus the dependence of τ_{el} on f is expected to be very weak in both cases for the Rouse model. For the Zimm model, with hydrodynamics, the situation is slightly different, $\tau_{el} \sim N^{3\nu} f^{(2-3\nu)/2}$.[15] For a good solvent, $\tau_{el} \sim N^{3\nu} f^{0.125}$.

Results for $C_R(t)$ for stars in a good and Θ solvent are presented in Figure 9 for three stars with $N = 100$. In agreement with earlier results of Grest *et al.*[14] for $N = 50$ in a very good solvent, the relaxation times τ_{el} for the elastic modes, which are determined by the slope at long times on this semilog plot, are essentially independent of f. Su *et al.*[30] found similar results for 3- and 4-arm stars using the bond-fluctuation method. This result that τ_{el} is nearly independent of f is in contrast with the independent strand model of Zimm and Kilb[16] which predicts that $\tau \sim f$. Even for undiluted stars, Boese *et al.*[57] found using dielectric relaxation that the relaxation

times of the end-to-end distance for *cis*-polyisoprene stars depended imperceptibly on f for $3 \leq f \leq 18$.

VI. Conclusions

In this paper, results from molecular dynamics simulations of many-arm star polymers in good, Θ, and poor solvents are presented. The results for a number of properties, including the mean-squared radius of gyration, the monomer density profiles, the distribution of center-to-end distances for the free end, and the relaxation of the shape fluctuations, agree very nickely with the scaling model first introduced by Daoud and Cotton[11] and Birshtein and Zhulina.[12] While this model, which assumes that each arm moves only in a well-defined cone, is clearly an oversimplification, it does a remarkably good job in predicting many of the properties of a dilute star. Why it works so well, particularly for the distribution of center-to-center distances of the free ends, is somewhat surprising and not well understood.[42]

The simulation results also compare very well with recent experiments on many-arm stars in dilute solution.[1-9] This is true, even though the simulated stars are for a simple coarse-grained model, in which niether bond bending nor torsional forces were included. By normalizing the results by those for a free chain of length N, the same as one of the arms of the star, the results for the simulated and experimental stars agree very well, particularly in a good solvent. The only observed discrepancy is for the mean-squared radius of gyration, $\langle R_G^2 \rangle$, in a Θ solvent, where the simulation results agree with experiments for polystyrene and polybutadiene stars but not polyisoprene for large f. All of the results agree for $f \lesssim 8$. Why the experimental data when normalized in the same way do not agree is not understood.

All of the results here are for a single star polymer in dilute solution. In order for the simulation to be feaible, the sovent was treated as a continuum and the resulting dynamics were those of the Rouse model in the free-draining limit. The next step is clearly to include solvent molecules explicitly. At present at least another order of magnitude in computer speed will be necessary for a serious study of the hydrodynamics of stars. Experimentally there are a number of interesting results[50,51] for which simulations can be very useful in helping to interpret when such simulations are more feasible.

Acknowledgment. I thank L. J. Fetters, K. Kremer, and T. A. Witten for helpful discussions and M. Murat for help with some of the analysis programs.

References and Notes

(1) Burchard, W. *Adv. Polym. Sci.* **1983**, *48*, 1.
(2) Roovers, J.; Bywater, S. *Macromolecules* **1972**, *5*, 385; **1974**, *7*, 443.
(3) Roovers, J.; Hadjichristidis, N.; Fetters, L. J. *Macromolecules* **1983**, *16*, 214. Huber, K.; Burchard, W.; Fetters, L. J. *Macromolecules* **1984**, *17*, 541.
(4) Toporowski, P. M.; Roovers, J. *J. Polym. Sci. Polym. Chem. Ed.* **1986**, *24*, 3009.
(5) Khasat, N.; Pennisi, R. W.; Hadjichristidis, N.; Fetters, L. J. *Macromolecules* **1988**, *21*, 1100.
(6) Bauer, B. J.; Fetters, L. J.; Graessley, W. W.; Hadjichristidis, N.; Quack, G. F. *Macromolecules* **1989**, *22*, 2337.
(7) Roovers, J.; Toporowski, P.; Martin, J. *Macromolecules* **1989**, *22*, 1897.
(8) Zhou, L.-L.; Hadjichristidis, N.; Toporowski, P. M.; Roovers, J. *Rubber Chem. Technol.* **1992**, *65*, 303.
(9) Roovers, J.; Zhou, L.-L.; Toporowski, P. M.; van der Zwan, M.; Iatrou, H.; Hadjichristidis, N. *Macromolecules* **1993**, *26*, 4324.
(10) de Gennes, P. G. *Scaling Concepts in Polymer Physics*; Cornell University Press: Ithaca, NY, 1979.
(11) Daoud, M.; Cotton, J. P. *J. Phys. (Paris)* **1982**, *43*, 531.
(12) Birshtein, T. M.; Zhulina, E. B. *Polymer* **1984**, *25*, 1453. Birshtein, T. M.; Zhulina, E. B.; Borisov, O. V. *Polymer* **1986**, *27*, 1078.
(13) Witten, T. A.; Pincus, P. *Macromolecules* **1986**, *19*, 2509.
(14) Grest, G. S.; Kremer, K.; Witten, T. A. *Macromolecules* **1987**, *20*, 1376.
(15) Grest, G. S.; Kremer, K.; Milner, S. T.; Witten, T. A. *Macromolecules* **1989**, *22*, 1904.
(16) Zimm, B. H.; Kilb, R. W. *J. Polym. Sci.* **1959**, *37*, 19.
(17) De'Bell, K.; Lookman, T. *Rev. Mod. Phys.* **1993**, *65*, 87.
(18) Lipson, J. E. G.; Whittington, S. G.; Wilkinson, M. K.; Martin, J. L.; Gaunt, D. S. *J. Phys. A* **1985**, *18*, L469. Wilkinson, M. K.; Gaunt, D. S.; Lipson, J. E. G.; Whittington, S. G. *J. Phys. A* **1986**, *19*, 789. Whittington, S. G.; Lipson, J. E. G.; Wilkinson, M. K.; Gaunt, D. S. *Macromolecules* **1986**, *19*, 1241.
(19) Ohno, K.; Binder, K. *J. Chem. Phys.* **1991**, *95*, 5444; **1991**, *95*, 5459.
(20) Miyake, A.; Freed, K. F. *Macromolecules* **1983**, *16*, 1228; **1984**, *17*, 678. Douglas, J. F.; Freed, K. F. *Macromolecules* **1984**, *17*, 1854.
(21) Vlahos, C. H.; Kosmas, M. K. *Polymer* **1984**, *25*, 1607.
(22) Duplantier, B. *Phys. Rev. Lett.* **1986**, *57*, 941; *Europhys. Lett.* **1988**, *8*, 677. Duplantier, B.; Saleur, H. *Phys. Rev. Lett.* **1986**, *57*, 3179; **1987**, *59*, 539.
(23) LeGuillou, J. C.; Zinn-Justin, J. *Phys. Rev. B.* **1980**, *21*, 3976.
(24) Raphaël, E.; Pincus, P.; Fredrickson, G. H. *Macromolecules* **1993**, *26*, 1996.
(25) Bishop, M.; Clarke, J. H. R. *J. Chem. Phys.* **1989**, *90*, 6647.
(26) Zimm, B. H. *Macromolecules* **1984**, *17*, 795.
(27) Freire, J. J.; Pla, J.; Rey, A.; Prats, R. *Macromolecules* **1986**, *19*, 452. Freire, J. J.; Rey, A.; de la Torre, J. G. *Macromolecules* **1986**, *19*, 457. Rey, A.; Freire, J. J.; de la Torre, J. G. *Macromolecules* **1987**, *20*, 342.
(28) Zifferer, G. *Makromol. Chem.* **1990**, *191*, 2717; *Makromol. Chem., Theory Simul.* **1992**, *1*, 55.
(29) Zifferer, G. *Makromol. Chem., Theory Simul.* **1993**, *2*, 653; *Macromol. Theory Simul.* **1994**, *3*, 163.
(30) Su, S.-J.; Denny, M. S.; Kovac, J. *Macromolecules* **1991**, *24*, 917. Su, S.-J.; Kovac, J.; *J. Phys. Chem.* **1992**, *86*, 3931.
(31) Sikorski, A. *Makromol. Chem., Theory Simul.* **1993**, *2*, 309.
(32) Mazur, J.; McCrackin, F. *Macromolecules* **1977**, *10*, 326.
(33) Kolinski, A.; Sikorski, A. *J. Polym. Sci., Polym. Chem. Ed.* **1982**, *20*, 3147; **1984**, *22*, 97.
(34) Barrett, A. J.; Tremain, D. L. *Macromolecules* **1987**, *20*, 1687.
(35) Batoulis, J.; Kremer, K. *Macromolecules* **1989**, *22*, 4277.
(36) Batoulis, J.; Kremer, K. *Europhys. Lett.* **1988**, *7*, 683.
(37) Bruns, W.; Carl, W. *Macromolecules* **1991**, *24*, 209.
(38) Siepmann, J. I.; Frenkel, D. *Mol. Phys.* **1992**, *75*, 59.
(39) Carmesin, I.; Kremer, K. *Macromolecules* **1989**, *21*, 2819; *J. Phys. (Paris)* **1990**, *51*, 915.
(40) Milchev, A.; Paul, W.; Binder, K. *J. Chem. Phys.* **1993**, *99*, 4786. Gerroff, I.; Milchev, A.; Paul, W.; Binder, K. *J. Chem. Phys.* **1993**, *98*, 6526.
(41) Grest, G. S.; Murat, M. In *Monte Carlo and Molecular Dynamics Simulations in Polymer Science*; Binder, K., Ed.; Clarendon Press: Oxford, U.K., 1994.
(42) Li, H.; Witten, T. A. *Macromolecules* **1994**, *27*, 449.
(43) Milner, S. T. *Science* **1991**, *251*, 905.
(44) Grest, G. S.; Murat, M. *Macromolecules* **1993**, *26*, 3108.
(45) Allen, M. P.; Tildesley, D. J. *Computer Simulation of Liquids*; Clarendon Press: Oxford, U.K., 1987.
(46) Grest, G. S.; Dünweg, B.; Kremer, K. *Comput. Phys. Commun.* **1989**, *55*, 269.
(47) Dan, N.; Tirrell, M. *Macromolecules* **1992**, *25*, 2890.
(48) Wijmans, C. M.; Zhulina, E. B. *Macromolecules* **1993**, *26*, 7214.
(49) Huber, K.; Burchard, W.; Bantle, S.; Fetters, L. J. *Polymer* **1987**, *28*, 1990; **1987**, *28*, 1997.
(50) Richter, D.; Stuhn, B.; Ewen, B.; Nerger, D. *Phys. Rev. Lett.* **1987**, *58*, 2462. Richter, D.; Farago, B.; Fetters, L. J.; Huang, J. S.; Ewen, B. *Macromolecules* **1990**, *23*, 1845.
(51) Richter, D.; Farago, B.; Huang, J. S.; Fetters, L. J.; Ewens, B. *Macromolecules* **1989**, *22*, 468.
(52) Boothroyd, A. T.; Squires, G. L.; Fetters, L. J.; Rennie, A. R.; Horton, J. C.; de Vallêra, A. M. B. G. *Macromolecules* **1989**, *22*, 3130.
(53) Dozier, W.; Huang, J. S.; Fetters, L. J. *Macromolecules* **1991**, *24*, 2810.
(54) Candau, F.; Rempp, P.; Benoit, H. *Macromolecules* **1972**, *5*, 627.
(55) Zimm, B. H.; Stockmayer, W. H. *J. Chem. Phys.* **1949**, *17*, 1301.
(56) Rosenbluth, A. W.; Rosenbluth, M. N. *J. Chem. Phys.* **1995**, *23*, 356.
(57) Boese, D.; Kremer, F.; Fetters, L. J. *Macromolecules* **1990**, *23*, 1826.